Citation: Molecular Therapy—Nucleic Acids (2015) 4, e235; doi:10.1038/mtna.2015.9

www.nature.com/mtna

Aptamer-Mediated Codelivery of Doxorubicin and NF-κB Decoy Enhances Chemosensitivity of Pancreatic Tumor Cells

David Porciani[1,2], Lorena Tedeschi[3], Laura Marchetti[1], Lorenzo Citti[3], Vincenzo Piazza[2], Fabio Beltram[1,2] and Giovanni Signore[2]

Aptamers able to bind efficiently cell-surface receptors differentially expressed in tumor and in healthy cells are emerging as powerful tools to perform targeted anticancer therapy. Here, we present a novel oligonucleotide chimera, composed by an RNA aptamer and a DNA decoy. Our assembly is able to (i) target tumor cells via an antitransferrin receptor RNA aptamer and (ii) perform selective codelivery of a chemotherapeutic drug (Doxorubicin) and of an inhibitor of a cell-survival factor, the nuclear factor κB decoy oligonucleotide. Both payloads are released under conditions found in endolysosomal compartments (low pH and reductive environment). Targeting and cytotoxicity of the oligonucleotidic chimera were assessed by confocal microscopy, cell viability, and Western blot analysis. These data indicated that the nuclear factor κB decoy does inhibit nuclear factor κB activity and ultimately leads to an increased therapeutic efficacy of Doxorubicin selectively in tumor cells.
Molecular Therapy—Nucleic Acids (2015) **4**, e235; doi:10.1038/mtna.2015.9; published online 28 April 2015
Subject Category: Aptamers, ribozymes and DNAzymes

Introduction

The therapeutic efficiency of chemotherapeutic agents is often hampered by their lack of selectivity.[1] A promising strategy to overcome these limitations relies on the engineering of systems for targeted delivery, *i.e.*, devices that can selectively recognize tumor cells and promote efficient internalization of the therapeutic payload, avoiding off-target toxicity. To this end, targeting of biomolecules overexpressed in tumor cells with natural or synthetic ligands (peptides, proteins, antibodies, aptamers) are actively explored.[2] One of the most promising targeting strategies involves the use of nucleic acid aptamers, short single-stranded oligonucleotides (DNA or RNA) able to recognize and bind their target molecule with high affinity and selectivity.[3,4] Compared with antibodies, aptamers are nonimmunogenic, easy to synthesize, optimize, and manipulate.[5] Furthermore, they can penetrate more efficiently into tumor tissues.[6] Recent studies led to the development of a variety of targeted drug-delivery platforms based on aptamer–drug conjugates (*e.g.*, aptamer–doxorubicin (Dox) conjugates)[7,8] or aptamer-nanomaterial assemblies.[9,10]

Here we focus on aptamers targeting transferrin receptor (TfR), a receptor which is overexpressed in many solid tumors.[11,12] These aptamers can bind human and mouse TfR either by showing higher affinity (*e.g.*, c2) or by targeting TfR in a different in different binding site with respect to transferrin (*e.g.*, FB4, GS24, and DW4).[13–15] Anti-TfR aptamers present a rather high potential, especially when selective delivery of anticancer agents with adverse side effects, such as Dox, is required. Dox is one of the most widely used chemotherapeutic drugs. Unfortunately, it shows rather significant unwanted cytotoxicity, especially toward cardiomiocytes.[16] In addition, its therapeutic efficiency sensibly decreases during the treatment because of acquired chemoresistance.[17]

Acquired chemoresistance was linked to activation of the nuclear factor *κB* (NF-κB),[18] a ubiquitous transcription factor that suppresses Dox-induced apoptosis.[1] NF-κB is activated in response to several stimuli (carcinogenesis, inflammatory agents, or chemotherapeutic drugs) and translocates from cytoplasm to the nucleus where it promotes transcription of antiapoptosis genes such as X-linked inhibitor of apoptosis protein (XIAP) and Bcl-2 family genes, ultimately conferring resistance toward apoptotic stimuli.[19] Recent studies demonstrated that inhibition of NF-κB sensitizes tumor cells to Dox-induced apoptosis in various cancer cells (breast cancer, pancreatic cancer, renal and hepatocellular carcinoma).[1,20,21] Several approaches were proposed to inhibit NF-κB activation;[1,19,22] among those, a decoy strategy that hampers binding of NF-κB to the promoter region of its targeted genes is a particularly reliable approach.[23,24] Decoys are synthetic, double-stranded oligonucleotides (ODNs) that selectively inhibit biological function of targeted transcription factors. NF-κB decoy ODNs are designed to mimic the κB consensus sequence recognized by NF-κB to the promoter regions of its target genes, ultimately preventing NF-κB binding to these sequences into the nucleus. The clinical application of this strategy is, however, limited by poor uptake into mammalian cells. This leads to the need for high dosage, repeated administrations, and long incubation times to obtain significant biological effects.[24]

Here we show our results on the design, synthesis, and optimization of an ODN chimera, named aptacoy, able to selectively target pancreatic tumor cells through a nuclease-stabilized anti-TfR RNA aptamer, and perform

[1]NEST, Scuola Normale Superiore and Istituto Nanoscienze-CNR, Pisa, Italy; [2]Center for Nanotechnology Innovation@NEST, Istituto Italiano di Tecnologia, Pisa, Italy; [3]CNR, Institute of Clinical Physiology, Pisa, Italy Correspondence: David Porciani, NEST, Scuola Normale Superiore and Istituto Nanoscienze-CNR, Piazza San Silvestro 12, Pisa 56127, Italy. E-mail: david.porciani@sns.it Or Giovanni Signore, Center for Nanotechnology Innovation@NEST, Istituto Italiano di Tecnologia, Piazza San Silvestro 12, Pisa 56127, Italy. E-mail: giovanni.signore@iit.it
Keywords: aptamer-decoy chimera; nucleic acid aptamer; aptamer-mediated codelivery; NF-kB decoy; targeted delivery
Received 15 August 2014; accepted 26 February 2015; published online 28 April 2015. doi:10.1038/mtna.2015.9

simultaneous, targeted release of Dox and NF-κB decoy, leading to highly targeted, synergistic effect of the two molecular payloads.

Results

Rational design of aptamer–Dox conjugate

It is known that Dox intercalates within DNA strands through its aromatic rings, preferentially binding to double stranded 5′-GC-3′ or 5′-CG-3′ sequences.[25] Our rational design of the therapeutic assembly started with the modification of a known anti-hTfR RNA aptamer (c2.min)[14] to increase its Dox-loading capacity. We designed an elongated aptamer bearing a short DNA tail $(CGA)_7$ at 3′end to create a duplex G-C rich region on hybridization with its complementary DNA sequence $(TCG)_7$, hereafter called antitail. Nucleic acid PACKage (NUPACK), a secondary structure prediction tool,[26] evidenced one Dox binding site on the RNA motif and six to seven possible binding sites on the duplex region of the oligonucleotidic carrier structure (hereafter c2C), yielding the potential for loading seven to eight Dox molecules/c2C (**Figure 1a**). Interestingly, the DNA duplex domain does not interfere with the correct RNA aptamer folding (**Figure 1a**), in agreement with previous findings involving similar structures.[27] Activity of c2C was assessed with a functional assay by monitoring internalization in pancreatic tumor cells (MIA PaCa-2) that overexpress hTfR.[28] The endocytosis process of the dual-labeled assembly (Atto 633 and Alexa Fluor 488 on c2.min and antitail portions of c2C, respectively) was monitored by confocal microscopy (**Figure 1b**). Complete colocalization of the two dyes in subcellular vesicles was observed after 20 minutes incubation, consistently with the uptake and retention of the entire complex.[29] Interestingly, considerable perinuclear localization was observed at longer times (120 minutes) for both dyes, suggesting that at least a fraction of c2C is not recycled during the endocytosis process. Overall, the endocytosis of the whole complex demonstrates the capability of c2.min to retain its activity even when embedded in a more complex ODN structure.

Next, we turned our attention to the assembly of a noncovalent conjugate between c2C and Dox. To this end, we evaluated Dox loading efficiency by monitoring quenching of its fluorescence emission on intercalation in DNA.[7] Dox fluorescence steadily decreased on incubation with the hybridized ODN for Dox/c2C ratios up to 7.5 : 1 (**Figure 1c**), in agreement with the predicted presence of seven to eight Dox binding sites (**Figure 1a**). Only low fluorescence reduction was detected in presence of c2.min and no quenching effect was observed in absence of the hybridization between the tail and antitail portions (see **Supplementary Figure S1**). This result confirms the role of the DNA duplex in Dox loading. Most importantly, c2C–Dox complex did not release Dox after 1 hour incubation in serum-containing medium (1% and 5%) at 37°C, and only minor leakage was observed (<10%) after

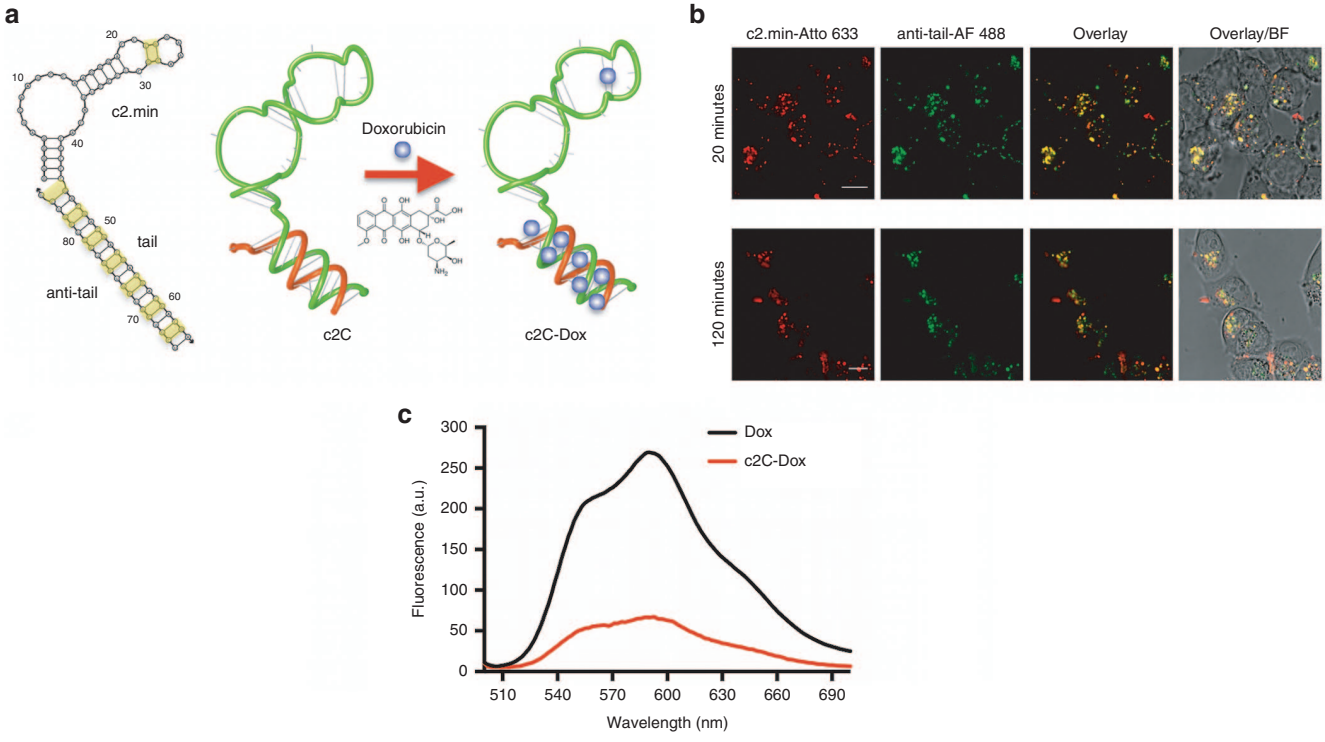

Figure 1 Rational design of c2C–Dox conjugate and internalization property in tumor cells of the dual-labeled ODN. (**a**) From left to right, secondary structure prediction of the hybridized assembly composed by the extended RNA aptamer (c2.min + tail) and antitail. Yellow boxes on the secondary structure indicate possible Dox binding sites within oligonucleotide structure. Note that each oligonucleotide is represented as an RNA sequence. (**b**) Cellular uptake of dual-labeled c2C (Alexa Fluor 488, green and ATTO 633, red) in pancreatic tumor cells (MIA PaCa-2). Extensive colocalization was observed both at early (20 minutes) and at longer (120 minutes) times. Scale bars: 10 μm. (**c**) Fluorescence spectra of free Dox solution (1.5 μmol/l) and c2C–Dox conjugate (7.5 molar ratio Dox/c2C); Dox fluorescence in the conjugated molecule is quenched because of its intercalation in DNA duplex.

2 hours incubation (see **Supplementary Table S1**). Notably, even with longer incubation (24 hours) the assembly was quite stable, and leakage from the double helix was ~25% in both serum conditions. In addition, no serum-concentration dependence was observed. This suggests that leakage occurs through thermally-driven Dox desorption from double helix that does not involve interaction with serum proteins.

Aptamer-mediated tumor targeting and antitumor efficacy of c2C–Dox

We next evaluated the aptamer-mediated uptake of Dox in tumor cells (MIA PaCa-2). Nontumoral mouse fibroblasts (NIH-3T3) were used as negative control.[30] Cells were treated with either the whole complex or free Dox, keeping constant both Dox concentration (1.5 μmol/l) and Dox/c2C ratio (7.5 : 1). After 2 hours incubation, confocal imaging microscopy showed that free Dox readily diffuses through the plasma membrane and accumulates into the nuclei of both hTfR-positive and hTfR-negative cells with nearly identical efficiency. In contrast, Dox internalization mediated by c2C was markedly different in tumor and control cells (**Figure 2**). Indeed, c2C–Dox was readily internalized in MIA PaCa-2 cells, as shown by Dox fluorescence detected both in endocytic vesicles and into the nucleus, whereas only a weak cytoplasmic signal was detected in control cells (NIH-3T3), likely because of negligible nonspecific internalization of the complex. Interestingly, uptake mechanisms for free Dox and c2C–Dox by MIA PaCa-2 cells appear quite different. Free Dox accumulates almost exclusively in the nuclear region, while c2C–Dox shows both nuclear fluorescence and cytoplasmic signal, in keeping with a subcellular compartimentalization of Dox within endosomes and lysosomes (endolysosomes) because of receptor-mediated endocytosis. This behavior is in agreement with previous studies that showed cytoplasmic localization of Dox released from transferrin–Dox conjugates.[31] The intracellular release of Dox from the ODN complex in MIA PaCa-2 cells was also evaluated at longer times (24 hours after treatment). Interestingly, higher fluorescence was observed both in the cytoplasm and in the nucleus (**Figure 2**). This fact suggests escape of Dox from DNA duplex during later stages of the endocytosis pathway.[32]

Next, we turned our attention to the assessment of c2C–Dox cytotoxic effects toward tumor cells using a cell viability assay (WST-8).[33]

Dose–response curves were recorded for both tumor and control cells treated with either free Dox or c2C–Dox. Furthermore, a c2-scrambled sequence (*i.e.*, c36) known not to recognize hTfR[14] was used as an additional control (c36C–Dox). A distinct cell line (HeLa) was also employed to assess the cytotoxicity of our complex with a different tumor model. As expected, Dox did present dose-dependent cytotoxicity in all cell lines. c2C–Dox was sensibly more selective, leading to higher cytotoxic effect both in MIA-PaCa-2 and in HeLa cells, when compared with controls (**Figure 3**). Notably, c36C–Dox did not show appreciable cytotoxicity in any tumor cell line, apart from a minor contribution likely stemming either from partial Dox leakage during incubation or some minor nonspecific uptake (**Figure 3**). This supports the observation that the observed cytotoxic enhancement shown by c2C–Dox is indeed related to an active targeting process. Interestingly, both free Dox and c2C–Dox showed higher cytotoxicity toward HeLa than MIA PaCa-2, indicating a higher Dox sensitivity of the cervical cancer cells when compared with the pancreatic tumor model.

Finally, we also confirmed that the observed cytotoxicity was actually related to an apoptotic process because of the intracellular Dox release, by means of an Annexin V/Propidium Iodide assay.[34,35] Treatment of MIA-PaCa-2 cells with c2C–Dox evidenced the typical pattern of late apoptotic cells. Conversely, treatment with free c2C did not induce appreciable fluorescence, indicating nonapoptotic cellular condition (see **Supplementary Figure S2**).

pH- and nuclease-dependent Dox release from the c2C–Dox

The release mechanism of Dox from DNA duplex during endocytosis pathway was investigated using simulated

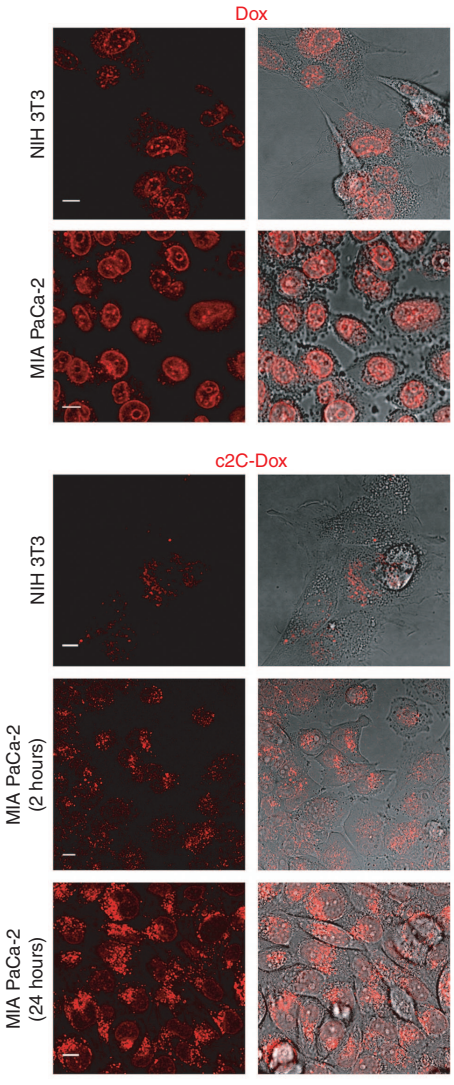

Figure 2 Selective internalization of the c2C–Dox conjugate in targeted tumor cells. Confocal imaging microscopy shows the intracellular distribution of free Dox and Dox released from c2C–Dox complex (red fluorescence) in tumor cells (MIA PaCa-2) and control cells (NIH-3T3). Scale bars: 10 μm.

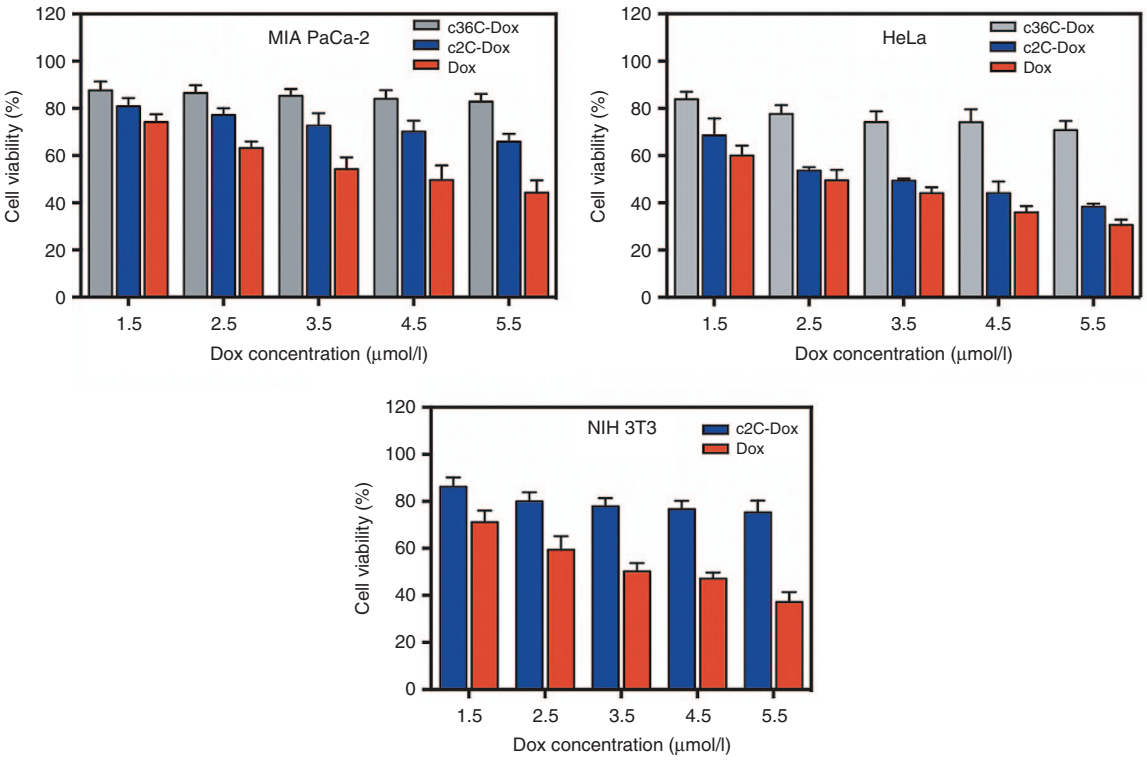

Figure 3 Cell viability assay of MIA PaCa-2, HeLa, and NIH-3T3 cells after treatment with free Dox (red), c2C–Dox (blue), and c36C–Dox (gray). Cells were incubated with the drugs for 2 hours and cell viability was assessed after 24 hours. Cell viability on incubation with c2C alone (see experimental part for further details) was 93.4 ± 2.0, 90.7 ± 2.6, and 88.7 ± 3.2 for MIA PaCa-2, HeLa, and NIH 3T3, respectively. Error bars represent the SD from three or more independent experiments.

conditions *in vitro*. c2C–Dox (1.5 μmol/l Dox concentration) was incubated in solutions at different pH (7.4, 6.5, 5.8, 5.5, 5.0), and fluorescence of the Dox released was compared with that of a Dox control sample at the same concentration.[36] Dox release increased at lower pH value, reaching 40% at pH 5.5 and 55% at pH 5.0 within 30 minutes (**Table 1**). Interestingly, this result is in excellent agreement with previous observations regarding Dox release in acidic solution.[37] On addition of DNA nucleases to c2C-Dox at pH 5.0, Dox release increased from 55% to 98% within 2 hours at room temperature. The observed pH dependency can be related to the protonation of $-NH_2$ groups on Dox at lower pH,[36] which reduces the hydrophobic interaction between the aromatic ring of Dox and the bases of DNA duplex. The pH- and nuclease-dependent Dox release from c2C–Dox conjugate is also consistent with the increased Dox fluorescence detected in cell cytoplasm at longer times (24 hours after treatment) (**Figure 2**) and supports the hypothesis of pH- and enzymatic Dox release at endolysosomal level during receptor-mediated endocytosis pathway.

Table 1 pH- and nuclease-triggered Dox release

pH	Doxorbicin released (%)[a]	SD
6.5	3.7	2.0
5.8	7.2	2.2
5.5	39.9	3.6
5.0	55.2	3.7
5.0[b]	101.3[c]	4.5

[a]Calculated by comparing fluorescence of free Dox at pH 7.4 (100%) with that of c2C–Dox samples on reaching equilibrium (30 minutes). [b]DNase I (2 μl, 2,000 U/ml) added. [c]After 2 hours incubation with DNase I.

Synthesis and Dox-loading of a novel aptacoy chimera

In order to increase the cytotoxicity of the c2C–Dox conjugate, we investigated a novel codelivery strategy. Recently, it was demonstrated that NF-κB activation suppresses the apoptotic potential of Dox, ultimately conferring an increased chemoresistance to a plethora of tumor cells.[1,18] Synthetic double-stranded DNA ODNs with high affinity for NF-κB, known as NF-κB decoys, were extensively used to block induction of gene expression mediated by NF-κB both *in vitro* and *in vivo*.[23,24] During translocation, NF-κB is potentially susceptible to hijacking by decoys bearing the binding sequence recognized by NF-κB.[38] Therefore, we designed a chimeric ODN, named aptacoy, composed by c2C portion directly conjugated to a NF-κB decoy. The latter portion mimics the κB consensus sequence for NF-κB binding and hampers its nuclear translocation, ultimately blocking the NF-κB-mediated downstream activation of antiapoptotic genes.

First, we designed a nuclease-resistant phosphorothioate ODN with a self-complementary sequence to obtain the suitable double-stranded DNA via intramolecular folding (see **Supplementary Figure S3**).[39] To promote release of NF-κB decoy from aptacoy after internalization in targeted cells, we conjugated NF-κB decoy with the antitail using a disulfide linker that is stable in the extracellular medium but is easily cleaved in reducing intracellular environment, such

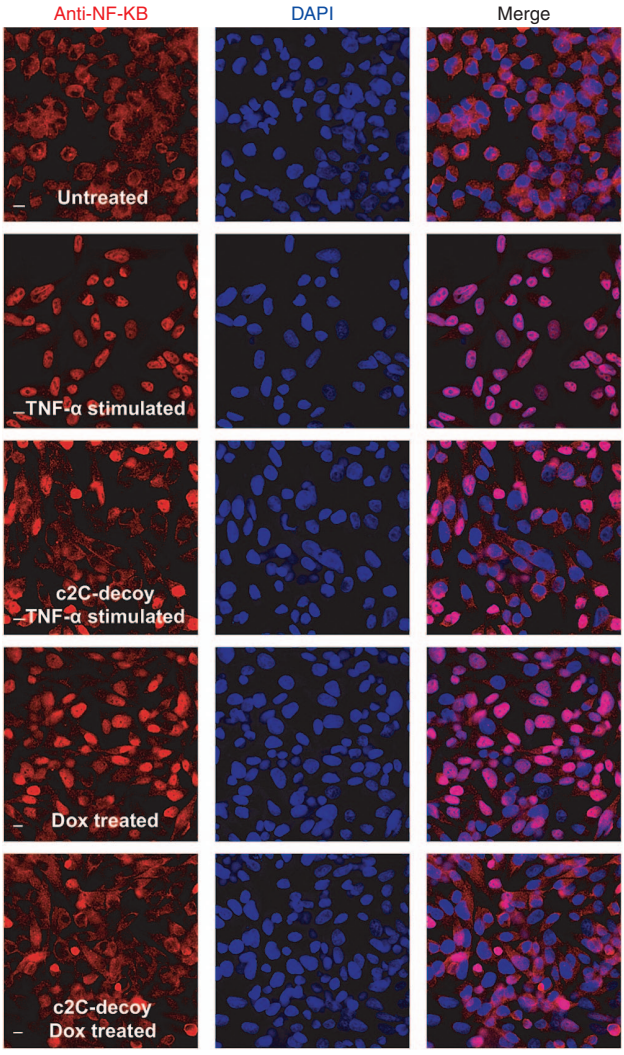

Figure 4 c2C–d conjugate inhibits NF-κB activity and sensitizes MIA PaCa-2 cells to Dox-induced apoptosis. Immunofluorescent staining of NF-κB assesses its cellular localization. MIA PaCA-2 cells were incubated with c2C-d or c2C alone for 24 hours and stimulated either with TNF-α (20 ng/ml) for 1 hour or with Dox for 24 hours before immunofluorescent staining of NF-κB (red). The nuclei were stained blue with DAPI. Scale bars = 10 μm.

as lysosomes.[40] The oligo conjugation was performed with a two-step procedure (see **Supplementary Figures S3 and S4**). After this process, the resulting conjugated product was hybridized with the tail portion of c2, to obtain the aptacoy structure, hereafter c2C-d. Incubation with a suitable amount of Dox yielded the final physical conjugate c2C-d–Dox (*i.e.*, aptacoy-Dox). Dox quenching because of intercalation within double-stranded DNA was comparable with our results with c2C–Dox (see **Supplementary Figure S5**). The presence of a double-stranded helix in the decoy domain of the construct may introduce additional sites for Dox intercalation. Thus, we added unconjugated NF-κB decoy to a Dox solution and monitored fluorescence intensity changes to assess the quenching effect of decoy. Originally, we detected a noticeable Dox fluorescence quenching, which however was remarkably smaller than that shown by hybridized complex (see **Supplementary Figure S5**). Overall, these results confirmed that maximum quenching effect was because of the formation of the aptacoy–Dox complex.

Despite the presence of additional binding sites, Dox/c2C-d molar ratio was kept constant at 7.5 in subsequent experiments to better compare therapeutic efficiency of both complexes (c2C–Dox versus c2C-d–Dox). Note, however, that greater Dox/c2C-d ratios are achievable by exploiting the additional binding sites present on the double-stranded decoy.

Codelivery of Dox and NF-κB decoy via anti-TfR aptamer in living cells

We investigated whether the NF-κB decoy could be effectively released in cytoplasm from the aptacoy, ultimately inhibiting the transcriptional activity of NF-κB. To this end, we performed fluorescence immunostaining of NF-κB in MIA PaCa-2 cells to monitor its cellular localization in different conditions.

In unstimulated MIA PaCa-2 cells (treated only with c2C), NF-κB was found mainly in the cell cytoplasm as confirmed by the lack of colocalization between NF-κB and nuclear marker DAPI (**Figure 4**). Stimulation with NF-κB inducer TNF-α (20 ng/ml) led to an impressive accumulation of NF-κB in cell nuclei, as shown by the complete colocalization between NF-κB and DAPI. Interestingly, nuclear translocation of NF-κB was significantly reduced in MIA PaCa-2 cells treated with c2C-d prior to TNF-α stimulation, as shown by cytoplasmic localization of NF-κB (**Figure 4**). The inhibition of TNF-α-induced NF-κB activation indicates that NF-κB decoy was actually released from c2C-d and could bind NF-κB in the cell cytoplasm hampering its nuclear translocation.[41] The actual mechanism of decoy endosomal escape is not quite clear, however, as is the case for most therapeutic ODNs (siRNAs, miRNAs, antagomirs, antisense oligos, and hammerhead ribozymes).[42,43]

Next, we evaluated the effect of Dox on NF-κB nuclear translocation in MIA PaCa-2 cells. Not surprisingly, MIA PaCa-2 cells showed a prominent nuclear translocation of NF-κB after Dox stimulation in agreement with previous studies on different cell lines.[20,21] However, treatment with c2C-d efficiently decreased Dox-induced NF-κB nuclear translocation, confirming the inhibitory activity exhibited by the decoy toward NF-κB (**Figure 4**).

Then, we evaluated whether c2C-Dox-d could improve sensitization of tumor cells to the apoptotic effect of released Dox. In order to compare the cytotoxicity of c2–Dox and c2C–Dox–d, we performed cell-viability assays on pancreatic tumor and control cells. In addition, we examined the behavior of c2C-sd–Dox, a construct bearing a scrambled decoy sequence[23] to assess the potential cytotoxicity of a phosphorothioate payload. Dose–response curves were obtained for each complex toward MIA PaCa-2 cells (**Figure 5a**). Cytotoxicity of c2C-d–Dox significantly exceeded values found for c2C–Dox, and was quite comparable with free Dox. Conversely, treatment with c2C-sd–Dox did produce effects identical to the administration of c2C-Dox, thus evidencing that increased cytotoxicity is related to the effect of the decoy itself (**Figure 5a**).

Furthermore, this complex fully retained its targeting properties, being able to deliver Dox selectively in targeted cells, as shown by the almost null cytotoxicity toward NIH-3T3 cells

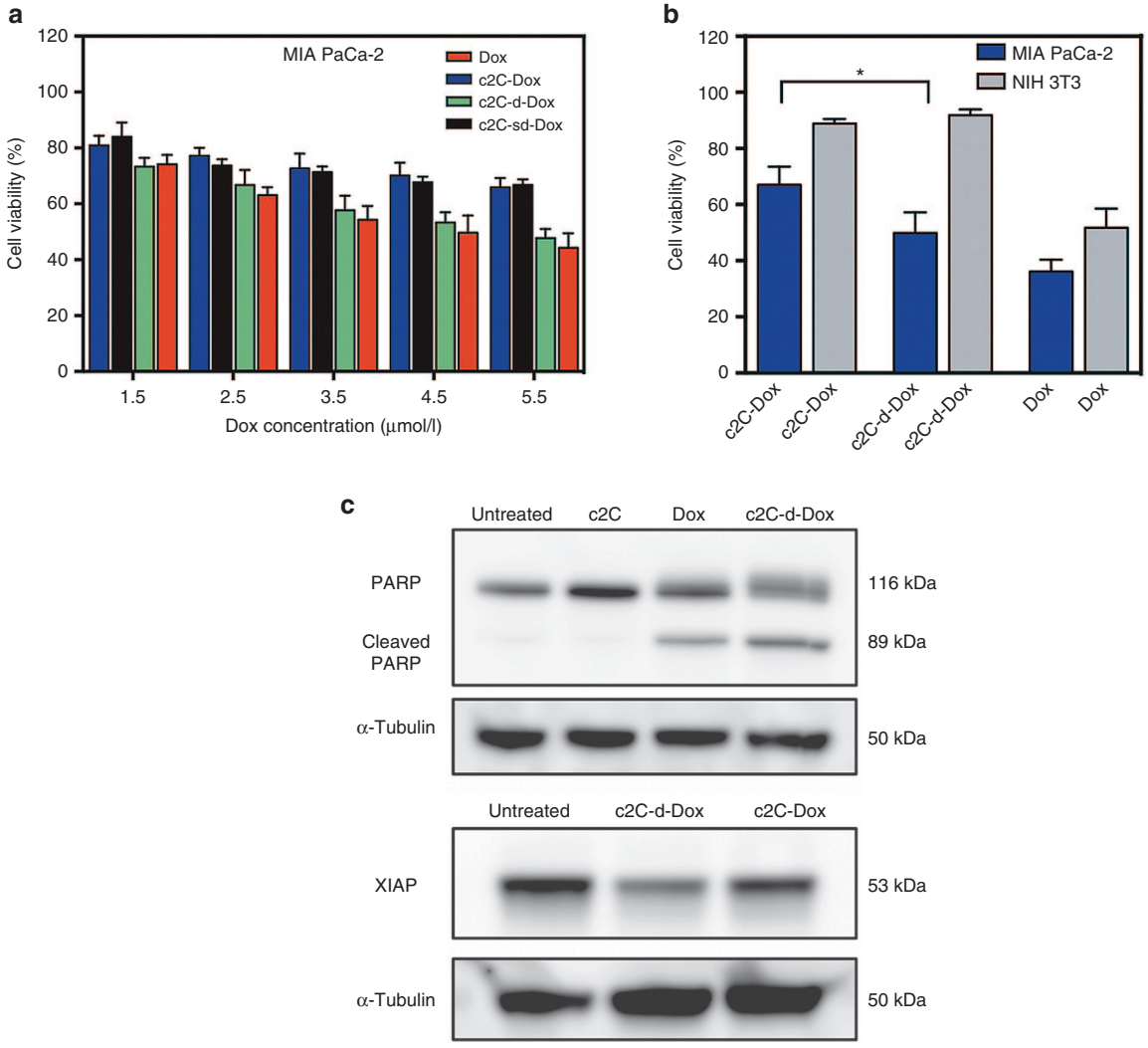

Figure 5 (**a**) Cell viability assay of MIA PaCa-2 cells after treatment with free Dox (red), c2C–Dox (blue), c2C-d–Dox (green) and c2C-sd–Dox (black). Cells were incubated with the drugs for 2 hours and cell viability was assessed after 24 hours. (**b**) Cell viability assay of MIA PaCa-2 (blue) and NIH-3T3 (gray) cells after treatment with free Dox, c2C–Dox, c2C-d–Dox or c2C for 24 hours. Error bars represent the SD from three or more independent experiments ($P < 0.05$). (**c**) Western blot analysis performed on MIA PaCa-2 cells using antibodies specific for PARP and XIAP. α-Tubulin was used as a loading control.

even on continuous treatment (24 hours) with the complex (**Figure 5b**).

Next, we sought to investigate whether the enhanced cytotoxic effect shown by aptacoy–Dox complex was actually because of an apoptotic process. To this end, Western blot analysis was performed to evaluate the extent of poly-(ADP-ribose) polymerase (PARP) cleavage, a well-established apoptotic marker.[44] PARP cleavage was observed on treatment with either free Dox or c2C-d–Dox (**Figure 5c**). On the contrary, resting cells and c2C-treated cells did not present significant accumulation of cleaved PARP. Notably, the relative intensity of cleaved versus full-length bands suggests that apoptotic processes are enhanced on treatment with c2C-d–Dox compared to free Dox. This important outcome suggests that the enhanced cytotoxicity of c2C-d–Dox observed with MIA PaCa-2 cells is indeed related to an increased apoptosis.

Finally, we investigated the expression of XIAP whose expression is tightly regulated by NF-κB. XIAP belongs to the family of inhibitor of apoptosis proteins and is directly involved in caspases inhibition to protect cell against death.[19] Enhanced NF-κB activity and consequently a marked up-regulation of XIAP were found in chemoresistant pancreatic cancer cells.[19,45]

Western blot analysis was performed to monitor XIAP expression in MIA PaCA-2 cells on treatment with c2C, c2C-Dox, or c2C-d-Dox. Importantly, a remarkable decrease of XIAP expression was observed in cells treated with c2C-d–Dox when compared with resting and c2C–Dox treated cells (**Figure 5c**). Notably, XIAP expression of resting cells exceeded what found for c2C–Dox, which in turn was higher than that relative to the c2C-d–Dox. This trend matches the reported repression of XIAP gene expression induced by Dox[46] which is significantly improved by

the effective inhibition of NF-κB activity after aptacoy–Dox treatment.

Overall, these results demonstrate that the combination of Dox and NF-κB decoy sensitizes pancreatic cancer cells, ultimately leading to the enhancement of Dox-mediated apoptotic effect.

Discussion

In summary, we presented a molecular-engineering strategy to design a drug-delivery platform composed uniquely by ODNs. This assembly exploits receptor-mediated internalization to perform selective delivery of Dox in tumor pancreatic cells and sensitizes them to Dox-induced apoptosis. We combined the targeting ability of an RNA aptamer that recognizes tumor cells expressing TfR and the inhibitory effect of a DNA decoy toward NF-κB. The complex was generated by DNA self-assembly between two complementary single-stranded DNA sequences: one located within targeting RNA aptamer and one covalently linked to NF-κB decoy with a disulfide bridge. The resulting aptacoy can accomodate multiple Dox molecules in DNA duplex domains yielding a therapeutically-active complex. We demonstrated that the aptamer motif promotes efficient selective delivery of molecular payloads in tumor cells. Most importantly, the codelivery of a decoy significantly increased Dox cytotoxicity toward targeted pancreatic tumor cells owing to selective inhibition of constitutive NF-κB activity. We believe that the present drug-delivery platform can lead to reduction of tumor chemoresistance toward Dox thus enhancing its therapeutic efficiency. Finally, the flexibility of our aptacoy platform represents a useful starting point for further engineering of this system with the intriguing possibility to design specific ODN architectures exploiting appropriate combinations of aptamer ligands, decoys, and drugs that could pave the way to the development of highly functional targeted therapy.

Materials and methods

Materials. All chemicals were purchased from Sigma Aldrich (St Louis, MO) unless otherwise specified, and were used as received. ODN synthesis and purification were performed according to a reported protocol.[47] High-performance liquid chromatography (HPLC) analyses, absorption, and fluorescence measurements were performed accorded to reported protocols.[13]

ODN sequences. All phosphoramidite monomers were purchased from Glen Research (Sterling, VA).

The sequence of the anti-TfR RNA aptamer (c2.min) with a short DNA tail $(CGA)_7$ at the 3′end was the following (tail sequence is in italic):

5′-GGGGGAUCAAUCCAAGGGACCCGGAAAC GCUCCCUUACACCCC*CGACGACGACGACGACGACGA*-3′

The sequence of the scrambled aptamer (c36) with a short DNA tail $(CGA)_7$ at the 3′end was the following (extended sequence of aptamer is in italic):

5′GGCGUAGUGAUUAUGAAUCGUGUGCUAAU ACACGCC*CGACGACGACGACGACGACGA*-3′

All pyrimidines of the RNA aptamer motif were substituted by 2′-fluoro-pyrimidines. All synthesized ODNs contained a 5′amino group attached by a C-6 alkyl chain.

The antitail sequence was the following: 5′-TCGTCG TCGTCGTCGTCGTCG-3’

The sequence of the phosphorothioate NF-κB decoy was the following (consensus sequence are in italic): 5′-CCT*GGAAAGTCCC*GAAA*GGGACTTTCC*AGG-3′

The sequence of scrambled phosphorothioate NF-κB decoy was the following (complementary sequences are in italic)

5′-*GCCGTACCTGACTTAGCC*GAAA*GGCTAA GTCAGGTACGGC*-3′

All synthesized phosphorothioate ODNs contained a 3′amino group attached by a C-6 alkyl chain.

Cell culture. Human pancreatic carcinoma cells (MIA PaCA-2), human cervical cancer cells (HeLa), and mouse embryonic fibroblast cells (NIH-3T3) were purchased from the American Type Culture Collection (ATCC, Manassas, VA). All cell lines were grown using a previously reported protocol.[13]

Confocal imaging of cells. Cells were imaged using a Leica TCS SP5 SMD inverted confocal microscope (Leica Microsystems, Heidelberg, Germany) interfaced with a diode laser (Picoquant, Berlin, Germany) for excitation at 405 nm, with Ar lasers for excitation at 488 and 561 nm and with a HeNe laser for excitation at 633 nm. Glass bottom Petri dishes containing cells were mounted in a thermostated chamber at 37°C (Leica Microsystems) and viewed with a 63×1.2 NA water immersion objective or 40×1.5 NA oil immersion objective (Leica Microsystems). The pinhole aperture was set to 1.0 Airy. All data collected were analyzed by ImageJ software version 1.44o.

Secondary structure and hybridization predictions. ODN secondary structure predictions were obtained using the Internet tool NUPACK nucleic acid package (http://www.nupack.org/) with the default settings. Hybridization prediction between the tail sequence on the RNA aptamer structure and its short DNA complementary sequence (antitail) were obtained with NUPACK analysis algorithms software, representing each ODN as an RNA sequence. The NUPACK-generated secondary structures were used to obtain three-dimensional structures exploiting the utilities of the NUPACK software.

ODN labeling. The amino residues at 5′-end of the extended RNA aptamer (c2.min + tail) and antitail were conjugated, to the ATTO 633 NHS fluorophore (ATTO-TEC GmbH, Siegen, Germany) and Alexa Fluor 488 NHS fluorophore (Invitrogen, Carlsbad, CA), respectively, by means of standard NHS coupling procedures between the primary amine of the ODNs and NHS-derivative of the fluorophores. The labeling reaction, purification, and quantification of the final product were performed according to a reported protocol.[13]

ODN annealing protocol. To assemble the extended sequence of the RNA aptamer with its complementary DNA sequence, these two ODNs were mixed with equal molar concentration in a buffer solution, (PBS 1X containing 1 mM $MgCl_2$). The mixture was placed in a thermoblock and heated

to 90°C for 1 minute to denature the nucleic acid structures. Then, the entire apparatus was placed on the workbench for 30 minutes and denatured oligo sample was slowly cooled to allow correct hybridization between the two complementary strands. The hybridized product was always freshly prepared before each evaluation.

Dox intercalation in double helix region of the hybridized aptamer. A physical conjugate between hybridized aptamer carrier sample (c2C, c36C, c2C-d, and c2C-sd) and Dox was made by addition of 1 : 7.5 molar ratio of aptamer to Dox in binding buffer (PBS 1× containing 1 mmol/l $MgCl_2$). Dox fluorescence was measured (excitation: 480 nm, emission: 500–700 nm). Slits for both excitation and emission were set at 10 nm. The resulting complex (c2C–Dox, c36C–Dox, c2C-d–Dox, and c2C-sd–Dox) was freshly prepared before each experiment.

Dox release from aptamer in serum-containing media. After physical conjugate preparation between c2C and Dox, the c2C–Dox complex was added to either 1% or 5% serum-containing medium and incubated at 37 °C for 0, 30, 60, 120 minutes, and 24 hours. Dox fluorescence was measured (excitation: 480 nm, emission: 540–700 nm. Slits for excitation and emission were set at 20 and 10 nm, respectively). The amount of Dox released was determined by comparison with that of a Dox sample incubated in the same conditions, assuming the fluorescence intensity of the starting complex and of free Dox sample as 0 and 100%, respectively.

Assessment of cellular uptake by confocal microscopy. Internalization assay in MIA PaCa-2 cells was performed using a dual-labeled conjugate, in which the extended c2.min was labeled with ATTO 633 and the antitail was labeled with Alexa Fluor 488. MIA PaCa-2 cells were seeded 24 hours before the experiment in WillCo dishes to reach 80–90% confluence. Standard conditions for incubation consisted in 15-minute incubation at 37°C, 5% CO_2 in DMEM containing 1% bovine serum albumin (BSA), 0.2 mg/ml calf thymus DNA, and 0.2 μM of dual-labeled probe in a total volume of 500 μl. After incubation, cells were washed three times with PBS, fresh serum-containing medium was added and the sample was imaged by confocal microscopy.

Cellular uptake of free Dox and c2C-Dox conjugate was assessed through confocal imaging evaluation both on MIA PaCa-2 cells and NIH-3T3 cells. In brief, the cells were seeded 24 hours before experiment in WillCo dishes to reach 80–90% confluence. Then, the cells were incubated with a 1% serum-containing medium with either free Dox or c2C-Dox (1.5 μmol/l Dox concentration) for 2 hours at 37 °C. After incubation, cells were washed three times with PBS, then fresh 1% serum-containing medium was added, and the sample was imaged by confocal microscopy either immediately (*i.e.*, after 2 hours of incubation) or after additional 22 hours of incubation with drug-free culture medium (*i.e.*, after 24 hours). Dox fluorescence in living cells was detected by confocal microscopy using 488 nm as excitation wavelength. All experiments were performed in triplicate.

WST-8 cell viability assay. Cytotoxicity of free Dox and aptamer–Dox complexes was evaluated by using a tetrazolium salt, 2-(2-methoxy-4-nitrophenyl)-3-(4-nitrophenyl)-5-(2,4-disulfophenyl)-2*H*tetrazolium, monosodium salt (WST-8) assay. MIA PaCA-2 cells, HeLa cells, and NIH-3T3 cells (1×10^4 cells per well) were seeded in 96-well plates. After culture for 24 hours, the cells were incubated with a 1% serum-containing medium with either free Dox or oligo-Dox conjugates for 2 hours. After 2 hours incubation, cells were washed twice with PBS and then fresh 1% serum-containing medium was added. After 24 hours from the treatment the medium was removed and cells were incubated with WST-8 reagent (10 μl) and 1% serum-containing medium (90 μl) for 3 hours. Dose–response curves for MIA PaCa-2, HeLa, and NIH 3T3 were obtained using increasing drug concentrations (1.5, 2.5, 3.5, 4.5, and 5.5 μmol/l as Dox concentration and 0.20, 0.33, 0.46, 0.6, 0.73 μmol/l as oligo concentration). The unconjugated aptamer cytotoxicity (c2C) was evaluated treating the cells with the higher aptamer concentration (0.73 μmol/l) employed in dose–response curve experiments. Absorbance (450 nm) was measured using a microplate reader (Infinite F50, Tecan, Männedorf, Switzerland). The percentage of cell viability was determined by comparing drug-treated cells with the untreated cells (100% viability). Data represent the average of three or more independent experiments. Error bars represent the SD from three or more independent experiments.

Statistical analysis. Data obtained from cell viability assay were statistically analyzed using one-way ANOVA followed by Tukey's HSD test for multiple comparison analysis. Data are expressed as mean with 95% confidence intervals for all groups. *P*-values <0.05 were considered statistically significant. Statistical analyses and graphs were assembled using GraphPad PRISM (version 6, GraphPad software for Science, San Diego, CA).

Apoptosis assay. Apoptosis evaluation was performed as described in what follows, using Alexa Fluor 488 annexin V/Dead Cell Apoptosis Kit (Life Technologies, Carlsbad, CA). Cells were seeded (2×10^5 cells per well) in Willco dishes. After culture for 24 hours, the cells were incubated with 1% serum-containing medium supplemented with either c2C–Dox conjugate (1.5 μmol/l Dox concentration) or free c2C (0.2 μmol/l aptamer concentration) as negative control for 24 hours. The subsequent procedures were performed in accordance with the manufacturer's protocol. Confocal microscopy was used to monitor qualitatively the cellular staining using a dual filter set for Alexa Fluor 488 and propidium iodide and a 40×1.5 NA oil immersion objective. Qualitative apoptosis evaluation was determined by comparing drug-treated cells with the untreated cells. The experiment was performed in duplicate with the acquisition of an elevated number of random regions of interest for each experiment.

pH- and nuclease-dependent drug controlled release. Dox release in cuvette was studied as follows: the c2C–Dox conjugate (1.5 μmol/l Dox concentration) was incubated into binding buffer solution (PBS containing 1 mmol/l $MgCl_2$) with

different pH values: 7.4, 6.5, 5.8, 5.5, or 5.0. pH values were adjusted by the addiction of different aliquots of HCl 1M to each sample. The samples were placed in a quartz cuvette, and Dox fluorescence was monitored in real time spectrophotometrically. The acquisition for each sample was completed when fluorescence intensity became stable. In order to mimic lysosomal environment, 2 µl of DNase I (2,000 units/ml; New England Biolabs, Ipswich, MA) were added to the c2C-Dox sample at pH 5.0, and the sample was incubated at room temperature. During this incubation, Dox fluorescence was recorded at regular time intervals (10–15 measurements/hour). Fluorescence of free Dox samples was measured for each pH value, and measured fluorescence changes were used to normalize signals detected for the c2C–Dox samples. Percentage of Dox released was calculated by comparing fluorescent signals of free Dox at pH 7.4 (100%) with the signals of the c2C–Dox samples. Data represent the average of two or more independent experiments. Error bars represent the SD from two or more independent experiments.

Synthesis of the NF-κB decoy–antitail conjugate. The amino residues at 3′-end of the NF-κB decoy were conjugated to the dithio-bis(succinimidyl propionate) using the following protocol: 10 nmol of decoy were dissolved in sodium bicarbonate buffer 0.15 mol/l at pH 8.5 and mixed with 40-fold molar excess (400 nmol, in 20 ml of DMSO) of dithio-bis(succinimidyl propionate) in a final volume of 200 µl. The reaction mixture was stirred overnight at 4 °C. Analytical evaluation of the chemical conjugation reaction was performed at 25 °C using RP-HPLC analysis. The derivatized decoy was purified from unreacted dithio-bis(succinimidyl propionate) by dialysis using dialysis membrane (MWCO 1000) (Spectrum Laboratories, Rancho Dominguez, CA), concentrated using centrifugal filter units (3 K MWCO) and quantified by UV–VIS analysis. Next, a two-step reaction was performed to conjugate the carboxyl residue of the linker on derivatized decoy with the amino group at 5′-end of the antitail. Carboxyl group was activated with EDC (1000-fold molar excess) and Sulfo-NHS (10-fold molar excess) in PBS buffer for 20 minutes. Then, 5′-amino-antitail (threefold molar excess) was added, and the reaction mixture was stirred 6 hours at room temperature in PBS buffer containing triethylamine 1 mmol/l at pH 7.8. Purification of the decoy–antitail conjugate was performed with an IE-HPLC on a DNA Pac PA200 4×250 mm (Thermo Scientific) at 1.0 ml/min, using Tris–HCl 20 mmol/l pH 9.5, ACN 10% (Eluent A), and $NaClO_4$ 400 mmol/l, Tris–HCl 20 mmol/l pH 9.5, ACN 10% (Eluent B) as mobile phase at 25 °C. Absorbance was measured between 200 and 650 nm. The desired product was separated by means of IE-HPLC from the excess of the antitail and collected. The collected fraction was then dialyzed using dialysis membrane (MWCO 1000), concentrated using centrifugal filter units (3 K MWCO), and quantified by UV–VIS analysis. Finally, an aliquot was analyzed in IE-HPLC to check the purity of desired product.

Detection of NF-κB by immunofluorescence staining of p65. Immunofluorescence staining on MIA PaCA-2 cells using an antibody against p65 subunit of NF-κB was performed as follows: rabbit polyclonal anti-NF-κB p65 (phospho S536, Abcam, Cambridge, UK) was used as primary antibody and the Alexa Fluor 647-donkey antirabbit IgG (H+L) antibody (Life Technologies, Carlsbad, CA) as secondary antibody.

Cells were seeded (2×10^5 cells per well) in Willco dishes. After culture for 24 hours, cells were incubated with 1% serum-containing medium supplemented with c2C–d conjugate or with c2C alone (0.2 µmol/l ODN concentration) as negative control for 24 hours. After this incubation, cells were treated with TNF-α (20 ng/ml) for 1 hour. In order to assess Dox effect on NF-κB nuclear translocation in the presence and the absence of the decoy, the cells were coincubated with Dox (1.5 µmol/l) either c2C-d or c2C alone as negative control for 24 hours.

Then, the cells were fixed with 4% paraformaldehyde and 4% sucrose in PBS (15 minutes, room temperature) and subsequently permeabilized with 0.25% triton X-100 (6–8 minutes, room temperature). After fixation and permeabilization treatment, the cells were incubated with a PBS solution containing 1% BSA as blocking agent (30 minutes, room temperature) before incubation with the primary antibody diluted 1 : 100 in 0.5% BSA/PBS (1 hour, room temperature). Next, the cells were washed three times with PBS and incubated with the secondary antibody diluted 1 : 150 in 0.5% BSA/PBS (45 minutes, dark, room temperature). Finally, the cells were mounted using Vectashield Mounting Medium with 4',6-diamidino-2-phenylindole (DAPI) (Vector Labs Burlingame, CA). Confocal microscopy was used to evaluate the cellular localization of NF-κB. The experiment was performed in duplicate with the acquisition of an elevated number of random regions of interest for each experiment.

Western blot analysis. MIA PaCa-2 cells were seeded (7×10^5 cells per well) in a six-well plate. After 24 hours, cells were incubated with 1% serum-containing medium supplemented with either free Dox or c2C-d–Dox or with c2C alone (1.5 and 0.2 µmol/l as Dox and ODN concentration, respectively) for PARP detection for 2 hours. Alternatively cells were treated with either c2C-d–Dox or c2C–Dox at the same conditions described above for XIAP detection. After 2 hours incubation, cells were washed twice with PBS then fresh 1% serum-containing medium was added. After 24 hours from the treatment the medium was removed and cells were washed in ice-cold PBS and lysed in RIPA buffer supplemented with proteases and phosphatases inhibitors (Roche, Basel, Switzerland). After clarification, each postnuclear supernatant was quantified for protein content by Bradford assay (Thermo Scientific, Waltham, MA), and 30 µg of each protein extract were resolved on 4–12% Criterion XT Bis–Tris gradient gel (Bio Rad, Hercules, CA). Proteins were electrotransferred to polyvinylidene difluoride membranes (Bio Rad). These were washed and blocked in TBST + 5% w/v either nonfat dry milk (recommended for PARP) or BSA (recommended for XIAP). The membranes were then incubated with either rabbit monoclonal antibody to PARP (1 : 1000 diluted, 9542, Cell Signaling Technology) or rabbit monoclonal antibody to XIAP (1 : 1000 diluted, 9770, Cell Signaling Technology) in blocking solution for 2 hours at room temperature. Immunodetection was performed using antirabbit horseradish peroxidase-linked secondary antibody (1 : 2,000 diluted, Cell Signaling Technology, Danvers, MA). Filters were developed using Clarity Western ECL substrate

(Biorad) and chemoluminescence signals detected by Image Quant LAS4000 (GE healthcare, Milan, Italy). The same membranes were also stripped and blotted against a rabbit monoclonal antibody to α-Tubulin (1 : 2000, clone B-512, Sigma) as loading control. Obtained images were subjected to linear contrast enhancement after image analysis.

Supplementary material

Figure S1 Fluorescence spectra of Dox solution (1.5 μM) incubated with: buffer, antitail, c2min, and c2C; Dox fluorescence in the conjugated (c2C–Dox) molecule is quenched because of its intercalation in DNA duplex.
Figure S2 Cell apoptosis assay. MIA PaCA-2 cells were incubated with Apt–Dox conjugate (1.5 μM Dox concentration) or aptamer alone (0.2 μM aptamer concentration) for 24 hours. Scale bars: 10 μm.
Figure S3 Synthesis of NF-κB decoy–antitail conjugate. On the top is depicted the secondary structure prediction of NF-κB. The yellow box highlights the consensus region recognized and bound by NF-κB. The first reaction is the conjugation of the DSP linker to the amino residues at 5′-end of the NF-κB decoy. Next, a two-step process affords the chemical conjugate between carboxyl residue of the linker on derivatized decoy and the amino group at 5′-end of the antitail. Purified conjugate was hybridized with the extended sequence of RNA aptamer to generate the Apt–decoy chimera (bottom) represented on the basis of its helicity.
Figure S4 HPLC traces of conjugation crude reaction mixture.
Figure S5 Dox quenching after intercalation with c2C, c2C–d, and decoy alone.
Table S1 Doxorubicin release from aptamer in serum-containing media.

Acknowledgments: The authors would like to thank Michela Serresi for useful discussions.

1. Nakanishi, C and Toi, M (2005). Nuclear factor-kappaB inhibitors as sensitizers to anticancer drugs. *Nat Rev Cancer* **5**: 297–309.
2. Yu, MK, Park, J and Jon, S (2012). Targeting strategies for multifunctional nanoparticles in cancer imaging and therapy. *Theranostics* **2**: 3–44.
3. Ellington, AD and Szostak, JW (1990). *In vitro* selection of RNA molecules that bind specific ligands. *Nature* **346**: 818–822.
4. Tuerk, C and Gold, L (1990). Systematic evolution of ligands by exponential enrichment: RNA ligands to bacteriophage T4 DNA polymerase. *Science* **249**: 505–510.
5. Keefe, AD, Pai, S and Ellington, A (2010). Aptamers as therapeutics. *Nat Rev Drug Discov* **9**: 537–550.
6. Hicke, BJ, Stephens, AW, Gould, T, Chang, YF, Lynott, CK, Heil, J *et al.* (2006). Tumor targeting by an aptamer. *J Nucl Med* **47**: 668–678.
7. Bagalkot, V, Farokhzad, OC, Langer, R and Jon, S (2006). An aptamer-doxorubicin physical conjugate as a novel targeted drug-delivery platform. *Angew Chem Int Ed Engl* **45**: 8149–8152.
8. Meng, L, Yang, L, Zhao, X, Zhang, L, Zhu, H, Liu, C *et al.* (2012). Targeted delivery of chemotherapy agents using a liver cancer-specific aptamer. *PLoS One* **7**: e33434.
9. Zhu, G, Zheng, J, Song, E, Donovan, M, Zhang, K, Liu, C *et al.* (2013). Self-assembled, aptamer-tethered DNA nanotrains for targeted transport of molecular drugs in cancer theranostics. *Proc Natl Acad Sci USA* **110**: 7998–8003.
10. Zhang, X, Chabot, D, Sultan, Y, Monreal, C and DeRosa, MC (2013). Target-molecule-triggered rupture of aptamer-encapsulated polyelectrolyte microcapsules. *ACS Appl Mater Interfaces* **5**: 5500–5507.
11. Daniels, TR, Delgado, T, Rodriguez, JA, Helguera, G and Penichet, ML (2006). The transferrin receptor part I: Biology and targeting with cytotoxic antibodies for the treatment of cancer. *Clin Immunol* **121**: 144–158.
12. Daniels, TR, Delgado, T, Helguera, G and Penichet, ML (2006). The transferrin receptor part II: targeted delivery of therapeutic agents into cancer cells. *Clin Immunol* **121**: 159–176.
13. Porciani, D, Signore, G, Marchetti, L, Mereghetti, P, Nifosì, R and Beltram, F (2014). Two interconvertible folds modulate the activity of a DNA aptamer against transferrin receptor. *Mol Ther Nucleic Acids* **3**: e144.
14. Wilner, SE, Wengerter, B, Maier, K, de Lourdes Borba Magalhães, M, Del Amo, DS, Pai, S *et al.* (2012). An RNA alternative to human transferrin: a new tool for targeting human cells. *Mol Ther Nucleic Acids* **1**: e21.
15. Chen, CH, Dellamaggiore, KR, Ouellette, CP, Sedano, CD, Lizadjohry, M, Chernis, GA *et al.* (2008). Aptamer-based endocytosis of a lysosomal enzyme. *Proc Natl Acad Sci USA* **105**: 15908–15913.
16. Menna, P, Salvatorelli, E and Minotti, G (2007). Doxorubicin degradation in cardiomyocytes. *J Pharmacol Exp Ther* **322**: 408–419.
17. Mi, J, Zhang, X, Rabbani, ZN, Liu, Y, Reddy, SK, Su, Z *et al.* (2008). RNA aptamer-targeted inhibition of NF-κ B suppresses non-small cell lung cancer resistance to doxorubicin. *Mol Ther* **16**: 66–73.
18. Bottero, V, Busuttil, V, Loubat, A, Magné, N, Fischel, JL, Milano, G *et al.* (2001). Activation of nuclear factor kappaB through the IKK complex by the topoisomerase poisons SN38 and doxorubicin: a brake to apoptosis in HeLa human carcinoma cells. *Cancer Res* **61**: 7785–7791.
19. Cao, LP, Song, JL, Yi, XP and Li, YX (2013). Double inhibition of NF-κB and XIAP via RNAi enhances the sensitivity of pancreatic cancer cells to gemcitabine. *Oncol Rep* **29**: 1659–1665.
20. Sims, JT, Ganguly, SS, Bennett, H, Friend, JW, Tepe, J and Plattner, R (2013). Imatinib reverses doxorubicin resistance by affecting activation of STAT3-dependent NF-κB and HSP27/p38/AKT pathways and by inhibiting ABCB1. *PLoS One* **8**: e55509.
21. Zhao, N, Wang, R, Zhou, L, Zhu, Y, Gong, J and Zhuang, SM (2014). MicroRNA-26b suppresses the NF-κB signaling and enhances the chemosensitivity of hepatocellular carcinoma cells by targeting TAK1 and TAB3. *Mol Cancer* **13**: 35.
22. Gilmore, TD and Herscovitch, M (2006). Inhibitors of NF-kappaB signaling: 785 and counting. *Oncogene* **25**: 6887–6899.
23. Shimizu, H, Nakagami, H, Tsukamoto, I, Morita, S, Kunugiza, Y, Tomita, T *et al.* (2006). NFkappaB decoy oligodeoxynucleotides ameliorates osteoporosis through inhibition of activation and differentiation of osteoclasts. *Gene Ther* **13**: 933–941.
24. De Stefano, D, De Rosa, G, Maiuri, MC, Ungaro, F, Quaglia, F, Iuvone, T *et al.* (2009). Oligonucleotide decoy to NF-kappaB slowly released from PLGA microspheres reduces chronic inflammation in rat. *Pharmacol Res* **60**: 33–40.
25. Chaires, JB, Herrera, JE and Waring, MJ (1990). Preferential binding of daunomycin to 5′ATCG and 5′ATGC sequences revealed by footprinting titration experiments. *Biochemistry* **29**: 6145–6153.
26. Zadeh, JN, Steenberg, CD, Bois, JS, Wolfe, BR, Pierce, MB, Khan, AR *et al.* (2011). NUPACK: Analysis and design of nucleic acid systems. *J Comput Chem* **32**: 170–173.
27. Kim, D, Jeong, YY and Jon, S (2010). A drug-loaded aptamer-gold nanoparticle bioconjugate for combined CT imaging and therapy of prostate cancer. *ACS Nano* **4**: 3689–3696.
28. Camp, ER, Wang, C, Little, EC, Watson, PM, Pirollo, KF, Rait, A *et al.* (2013). Transferrin receptor targeting nanomedicine delivering wild-type p53 gene sensitizes pancreatic cancer to gemcitabine therapy. *Cancer Gene Ther* **20**: 222–228.
29. Boyacioglu, O, Stuart, CH, Kulik, G and Gmeiner, WH (2013). Dimeric DNA aptamer complexes for high-capacity-targeted drug delivery using pH-sensitive covalent linkages. *Mol Ther Nucleic Acids* **2**: e107.
30. Bonmati-Carrion, MA, Alvarez-Sánchez, N, Hardeland, R, Madrid, JA and Rol, MA (2013). A comparison of B16 melanoma cells and 3T3 fibroblasts concerning cell viability and ROS production in the presence of melatonin, tested over a wide Range of Concentrations. *Int J Mol Sci* **14**: 3901–3920.
31. Kratz, F, Beyer, U, Roth, T, Tarasova, N, Collery, P, Lechenault, F *et al.* (1998). Transferrin conjugates of doxorubicin: synthesis, characterization, cellular uptake, and *in vitro* efficacy. *J Pharm Sci* **87**: 338–346.
32. Mo, R, Jiang, T, DiSanto, R, Tai, W and Gu, Z (2014). ATP-triggered anticancer drug delivery. *Nat Commun* **5**: 3364.
33. Inoue, S, Setoyama, Y and Odaka, A (2014). Doxorubicin treatment induces tumor cell death followed by immunomodulation in a murine neuroblastoma model. *Exp Ther Med* **7**: 703–708.
34. Vermes, I, Haanen, C, Steffens-Nakken, H and Reutelingsperger, C (1995). A novel assay for apoptosis. Flow cytometric detection of phosphatidylserine expression on early apoptotic cells using fluorescein labelled Annexin V. *J Immunol Methods* **184**: 39–51.
35. Carlo, R and Ildo, N (2006). Analysis of apoptosis by propidium iodide staining and flow cytometry. *Nat Protoc* **1**: 1458–1461.
36. You, J, Zhang, G and Li, C (2010). Exceptionally high payload of doxorubicin in hollow gold nanospheres for near-infrared light-triggered drug release. *ACS Nano* **4**: 1033–1041.
37. Wu, C, Han, D, Chen, T and Peng, L (2013). Building a multifunctional aptamer-based DNA nanoassembly for targeted cancer therapy. *J Am Chem Soc* **135**: 18644–18650.
38. Cooper, JA Jr, Parks, JM, Carcelen, R, Kahlon, SS, Sheffield, M and Culbreth, R (2000). Attenuation of interleukin-8 production by inhibiting nuclear factor-kappaB translocation using decoy oligonucleotides. *Biochem Pharmacol* **59**: 605–613.
39. Giannetti, A, Citti, L, Domenici, C, Tedeschi, L, Baldini, F, Wabuyele, MB, *et al.* (2006). FRET-based protein–DNA binding assay for detection of active NF-κB. *Sensors Actuators B Chem* **113**: 649–654.

40. Yang, J, Chen, H, Vlahov, IR, Cheng, JX and Low, PS (2006). Evaluation of disulfide reduction during receptor-mediated endocytosis by using FRET imaging. *Proc Natl Acad Sci USA* **103**: 13872–13877.
41. Shibuya, T, Takei, Y, Hirose, M, Ikejima, K, Enomoto, N, Maruyama, A *et al.* (2002). A double-strand decoy DNA oligomer for NF-kappaB inhibits TNFalpha-induced ICAM-1 expression in sinusoidal endothelial cells. *Biochem Biophys Res Commun* **298**: 10–16.
42. Esposito, CL, Cerchia, L, Catuogno, S, De Vita, G, Dassie, JP, Santamaria, G *et al.* (2014). Multifunctional aptamer-miRNA conjugates for targeted cancer therapy. *Mol Ther* **22**: 1151–1163.
43. Zhou, J, Bobbin, ML, Burnett, JC and Rossi, JJ (2012). Current progress of RNA aptamer-based therapeutics. *Front Genet* **3**: 234.
44. Boulares, AH, Yakovlev, AG, Ivanova, V, Stoica, BA, Wang, G, Iyer, S *et al.* (1999). Role of poly(ADP-ribose) polymerase (PARP) cleavage in apoptosis. Caspase 3-resistant PARP mutant increases rates of apoptosis in transfected cells. *J Biol Chem* **274**: 22932–22940.
45. Lopes, RB, Gangeswaran, R, McNeish, IA, Wang, Y and Lemoine, NR (2007). Expression of the IAP protein family is dysregulated in pancreatic cancer cells and is important for resistance to chemotherapy. *Int J Cancer* **120**: 2344–2352.
46. Bednarski, BK, Baldwin, AS Jr and Kim, HJ (2009). Addressing reported proapoptotic functions of NF-kappaB: targeted inhibition of canonical NF-kappaB enhances the apoptotic effects of doxorubicin. *PLoS One* **4**: e6992.
47. Tedeschi, L, Citti, L and Domenici, C (2005). An integrated approach for the design and synthesis of oligonucleotide probes and their interfacing to a QCM-based RNA biosensor. *Biosens Bioelectron* **20**: 2376–2385.

Supplementary Information accompanies this paper on the Molecular Therapy–Nucleic Acids website (http://www.nature.com/mtna)